Quantifying the effect of overland flow on Escherichia coli pulses during floods: use of a tracer-based approach in an erosion-prone tropical catchment

Laurie Boithias, Olivier Ribolzi, Guillaume Lacombe, Chanthamousone
Thammahacksa, Norbert Silvera, Keooudone Latsachack, Bounsamay
Soulileuth, Marion Viguier, Yves Auda, Elodie Robert, et al.

HAL Id: hal-03093896
https://hal.science/hal-03093896

Quantifying the effect of overland flow on *Escherichia coli* pulses during floods: use of a tracer-based approach in an erosion-prone tropical catchment

Laurie BOITHIAS[1,*], Olivier RIBOLZI[1], Guillaume LACOMBE[2], Chanthamousone THAMMAHACKSA[3], Norbert

SILVERA[4], Keooudone LATSACHACK[3], Bounsamay SOULILEUTH[3], Marion VIGUIER[3], Yves AUDA[1], Elodie

ROBERT[1], Olivier EVRARD[5], Sylvain HUON[4], Thomas POMMIER[6], Cyril ZOUITEN[1], Oloth

SENGTAHEUANGHOUNG[7], Emma ROCHELLE-NEWALL[4]

[1] Géosciences Environnement Toulouse, Université de Toulouse, CNES, CNRS, IRD, UPS, France

[2] CIRAD, UMR G-EAU, F-34398 Montpellier, France
G-EAU, Univ Montpellier, AgroParisTech, CIRAD, INRAE, Institut Agro, IRD, Montpellier, France

[3] IRD, Department of Agricultural Land Management (DALaM), P.O. Box 4199, Ban Nogviengkham, Xaythany District, Vientiane, Lao PDR

[4] Institute of Ecology and Environmental Sciences of Paris (iEES-Paris), Sorbonne Université, Univ Paris Est Creteil, IRD, CNRS, INRA, 4 place Jussieu, 75005 Paris, France

[5] Laboratoire des Sciences du Climat et de l'Environnement (LSCE/IPSL), Unité Mixte de Recherche 8212 (CEA/CNRS/UVSQ), Université Paris-Saclay, Gif-sur-Yvette, France

[6] Laboratoire d'Ecologie Microbienne, UMR1418 INRA, UMR 5557 CNRS, UCBL, VetAgroSup, Université de Lyon, Villeurbanne, France

[7] Department of Agricultural Land Management (DALaM), P.O. Box 4195, Ban Nogviengkham, Xaythany District, Vientiane, Lao PDR

* Corresponding author: laurie.boithias@get.omp.eu

27   Abstract

28   Bacterial pathogens in surface waters threaten human health. The health risk is especially high in

29   developing countries where sanitation systems are often lacking or deficient. Considering twelve flash-

30   flood events sampled from 2011 to 2015 at the outlet of a 60-ha tropical montane headwater catchment

31   in Northern Lao PDR, and using *Escherichia coli* as a fecal indicator bacteria, our objective was to quantify

32   the contributions of both surface runoff and sub-surface flow to the in-stream concentration of *E. coli*

33   during flood events, by (1) investigating *E. coli* dynamics during flood events and among flood events and

34   (2) designing and comparing simple statistical and mixing models to predict *E. coli* concentration in

35   stream flow during flood events. We found that in-stream *E. coli* concentration is high regardless of the

36   contributions of both surface runoff and sub-surface flow to the flood event. However, we measured the

37   highest concentration of *E. coli* during the flood events that are predominantly driven by surface runoff.

38   This indicates that surface runoff, and causatively soil surface erosion, are the primary drivers of in-

39   stream *E. coli* contamination. This was further confirmed by the step-wise regression applied to

40   instantaneous *E. coli* concentration measured in individual water samples collected during the flood

41   events, and by the three models applied to each flood event (linear model, partial least square model,

42   and mixing model). The three models showed that the percentage of surface runoff in stream flow was

43   the best predictor of the flood event mean *E. coli* concentration. The mixing model yielded a Nash-

44   Sutcliffe efficiency of 0.65 and showed that on average, 89% of the in-stream concentration of *E. coli*

45   resulted from surface runoff, while the overall contribution of surface runoff to the stream flow was

46   41%. We also showed that stream flow turbidity and *E. coli* concentration were positively correlated, but

47   that turbidity was not a strong predictor of *E. coli* concentration during flood events. These findings will

48   help building adequate catchment-scale models to predict *E. coli* fate and transport, and mapping the

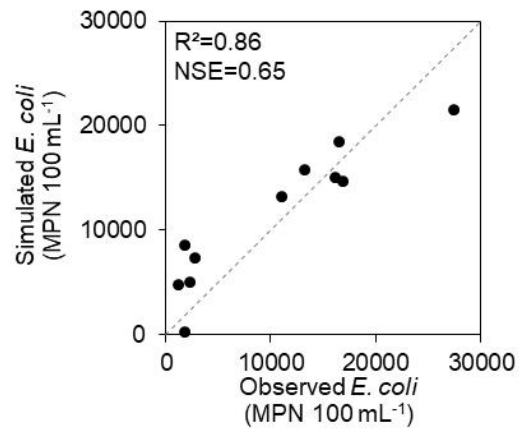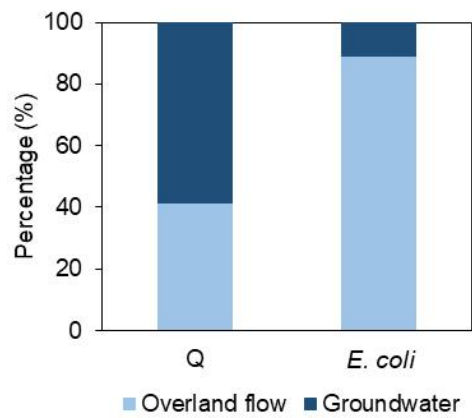49   related risk of fecal contamination in a global changing context.

50

54

55 **Graphical abstract**

56

57

1. Introduction

The presence of bacterial pathogens in surface waters threatens human health. Pathogenic bacteria are etiological agents of several waterborne diseases such as diarrhea, which is globally a leading cause of death among all ages (1.31 million deaths in 2015) (Troeger et al., 2017). These bacterial pathogens can be of fecal origin, e.g. from cattle or from human feces where open defecation is practiced or where sanitation systems are lacking or deficient (Exley et al., 2015; Tong et al., 2016). In developing countries, untreated surface water is often used for drinking, cooking, bathing and washing, thus exposing the population to a high health risk (Boithias et al., 2016).

Catchment microbial response depends on complex interactions between spatial patterns of land use, soil types, antecedent conditions of soil, and rainfall characteristics (Kim et al., 2018; McKergow and Davies-Colley, 2010; Pachepsky et al., 2018; Strauch et al., 2014). In the tropics, the presence in stream water of Fecal Indicator Bacteria (FIB), such as *Escherichia coli* (*E. coli*), is known to be partly driven by surface runoff (Causse et al., 2015; Ribolzi et al., 2016a) and groundwater flow (Chuah and Ziegler, 2018). However, the underlying mechanisms of FIB dynamics during storms remain to be fully documented. For example, there is a need to better quantify the respective contributions of surface and sub-surface flows to stream flow (e.g. using geochemical tracers) to understand and model the transfers of *E. coli* at the catchment scale during a flood event (Cho et al., 2016; Kim et al., 2017) and to predict the relative contributions of surface and sub-surface flows to the overall in-stream *E. coli* contamination (Chin, 2011).

E. coli is known to be transported in water as free cells or cells attached to particles of soil, manure or sediment (Garcia-Armisen and Servais, 2009; Krometis et al., 2007; Soupir et al., 2010). While stream flow turbidity is often higher in tropical areas, as compared to temperate areas, suspended sediments are known to carry *E. coli* (Nguyen et al., 2016). However, the relationships between stream flow turbidity, suspended sediments concentration, and *E. coli* concentration, and their possible hysteretic patterns during flood events, have not been yet fully explored.

4

82   Several studies in the tropics have investigated the relationships between suspended sediments

83   concentration and turbidity in rivers and lakes (Martinez et al., 2009; Robert et al., 2017, 2016; Ziegler et

84   al., 2014), and few studies investigated the relationships between suspended sediments concentration

85   and *E. coli* concentration (Boithias et al., 2016; Nguyen et al., 2016). However, to our knowledge, no

86   study has yet investigated the relationships between turbidity and *E. coli* concentration. Given that in-

87   stream *E. coli* concentration can vary rapidly during a flood event, a high-frequency sampling is required

88   to characterize this variability. The latter is both time consuming and expensive. Therefore, a proxy-

89   based approach is required and there is a need to verify if stream flow turbidity can be used as a proxy of

90   *E. coli* concentration during flood events.

91   In rural Southeast Asia, such as the uplands of Northern Lao PDR, livestock grazing and the lack of

92   adequate sanitation systems result in high levels of fecal contamination in surface waters during both

93   high and low flow seasons (Boithias et al., 2016; Nguyen et al., 2016; Rochelle-Newall et al., 2016). In

94   addition, Northern Lao PDR, like other mountainous regions in South-East Asia, is experiencing rapid

95   changes in land use (Ribolzi et al., 2017; Turkelboom et al., 2008). Annual crops are replaced by tree

96   plantations (e.g. teak) with limited understorey and litter coverage. This land-use change decreases soil

97   water infiltration and increases surface runoff and soil erosion (Lacombe et al., 2018; Ribolzi et al., 2017;

98   Song et al., 2020; Ziegler et al., 2004), but its impact on bacteria export has not yet been investigated.

99   Considering twelve flash-flood events sampled from 2011 to 2015 at the outlet of a 60-ha montane

100 tropical headwater catchment in Northern Lao PDR, our objective was thus to quantify the contributions

101 of both surface runoff and sub-surface flow to the in-stream concentration of *E. coli* during flood events,

102 by (1) investigating *E. coli* dynamics during flood events and among flood events and (2) designing and

103 comparing simple statistical and mixing models to predict *E. coli* concentration in stream flow during

104 flood events.

2. Materials and methods

2.1. Study design

In this paper, we quantify the relative roles of both surface runoff and sub-surface flow in the contamination of stream water by *E. coli* in a tropical montane catchment. To do so, we measured fine temporal-scale discharge and stream flow electrical conductivity to calculate the relative contributions of surface runoff and sub-surface flow to total stream flow. For twelve flash-flood events from 2011 to 2015 (named with the letters A to L), we then investigated statistical relationships between surface runoff, sub-surface flow, *E. coli* concentration, together with turbidity, total suspended sediments concentration, land-use features (areal percentage of land cover and *E. coli* input), and flood event-integrated variables, i.e. total rainfall, maximum rainfall intensity, rainfall duration, soil antecedent conditions, peak discharge, total volume of stream water exported during the flood event, and flow coefficient. For each flood event, we applied a mixing model to calculate the relative contributions of surface runoff and of sub-surface flow to the overall in-stream contamination by *E. coli*, by assigning to each one of these two flow components a characteristic bacteria concentration based on *E. coli* measurements in overland flow (overland flow *E. coli* end-member) and in groundwater (groundwater *E. coli* end-member).

2.2. Study area: the Houay Pano catchment

The 0.6 km^2 Houay Pano headwater catchment is located 10 km south of Luang Prabang city in Northern Lao PDR (Fig. 1a), within the 800 000 km^2 Mekong basin. This experimental site (Boithias et al., 2020) is part of the critical zone observatories' network named Multiscale TROPIcal CatchmentS (M-TROPICS), which belongs to the French Research Infrastructure OZCAR (Gaillardet et al., 2018). This catchment can be considered as being representative of the montane agro-ecosystems of South-East Asia. The climate is sub-tropical humid and is characterized by a monsoon regime with a dry season from November to May, and a wet season from June to October. The mean annual (2001-2019) temperature is 23.4 °C while the

129   mean annual rainfall is 1 366 mm (CV=0.23), about 71 % (CV=0.09) of which falls during the wet season.

130   Altitude within the catchment is 435-716 m (Fig. 1b) and the slope gradient is 1-135 % (mean=52 %). The

131   Laksip village, located downstream the S4 station (Fig. 1b), includes 484 inhabitants (Census of 2015).

2.3. Land use and land-use change

133   Detailed land-cover surveys and mapping were conducted each year from 2011 to 2015 within the

134   catchment (Boithias et al., 2020). The annual areal percentages of fallow (Fallow), teak trees (Teak),

135   annual crops (Annual crop), and annual crops grown under young teak trees (Teak+Crop) were calculated

136   using QGIS 2.6. We assessed the monthly *E. coli* input from 2011 to 2015 within the catchment with the

137   monthly counting of human and domestic animal (swine and poultry) traffic within the catchment, with

138   the daily feces production of humans and domestic animals, and with the *E. coli* content in their feces

139   (Causse et al., 2015).

2.4. Rainfall measurements

141   Rainfall was measured by an automatic weather station (Campbell BWS200 equipped with ARG100, 0.2

142   mm capacity tipping-bucket) located within the catchment (Fig. 1b). Data was recorded at 6-min time

143   interval from 2011 to 2012, and at 1-min time interval from 2013 to 2015. Data from 2013 to 2015 was

144   then cumulated into a 6-min time series for consistency with the 2011-2012 sub-period.

2.5. Flow rate measurements and water quality monitoring

146   We measured stream water level at the S4 gauging station of the catchment outlet (Fig. 1b) within a V-

147   notch weir equipped with a water level recorder (OTT Thalimedes) connected to a data logger, with 1-

148   mm vertical precision at a minimum of 3-min time interval. To relate water level to discharge, a control

149   rating curve was determined using both the velocity area method and the salt dilution method by slug

150   injection. Samples of stream water were collected at S4 gauging station in clean, plastic bottles using an

151   automatic sampler (Automatic Pumping Type Sediment Sampler, ICRISAT) for the measurement of Total

152   Suspended Sediments concentration ([TSS]), turbidity (Turbidity), Electrical Conductivity at 25°C (EC), and

153   *E. coli* concentration ([*E. coli*]). The automatic sampler was triggered by the water level recorder to

154   collect water after every 2-cm water level change during flood rising and every 5-cm water level change

155   during flood recession.

156   [TSS] was measured in each sample after filtration on 0.2 μm porosity cellulose acetate filters (Sartorius)

157   and evaporation at 105 °C for 48 h. Turbidity was determined with a turbidity meter (EUTECH

158   Instruments TN-100) and EC with a conductivity meter (WTW340).

159   For nine flood events (events A, B, F-L), we measured [*E. coli*] with the standardized microplate method

160   (ISO 9308-3). A water sub-sample was incubated at four dilution rates (i.e. 1:2, 1:20, 1:200 and 1:2000) in

161   a 96-well microplate (MUG/EC, BIOKAR DIAGNOSTICS) for 48 h at 44 °C. Ringers' Lactate solution was

162   used for the dilutions and one plate was used per sample. The number of positive wells for each

163   microplate was noted and the Most Probable Number (MPN) per 100 mL was determined using the

164   Poisson distribution. For three flood events (events C-E), we measured [*E. coli*] following the membrane-

165   filter method (EPA Method 1603). A small quantity of each water sample was filtered through the filter

166   membrane, which retained the bacterial cells. After filtration, this membrane was placed on a selective

167   medium (Sartorius NKS Endo nutrient pads), and incubated at 44 °C for 24 h. Shiny green *E. coli* colonies

168   were directly counted and expressed as Colony Forming Units (CFU) per 100 mL. Although "colony

169   forming unit" techniques and "most probable number" techniques are known to give highly correlated

170   results (e.g. Cho et al., 2010; Lušić et al., 2016; Wohlsen et al., 2006), we previously ensured that the two

171   methods were consistent in the Houay Pano catchment conditions (unpublished work).

172   In addition, we monitored surface runoff in the different land uses of the catchment from 2011 to 2015

173   using 1-m² microplots (Patin et al., 2018). We annually installed between 6 and 29 microplots to collect

174   surface runoff water samples during each rainfall event and to measure EC with WTW340. In 2012 and

175   2014, we used sub-samples of surface runoff water to measure *E. coli* concentration in surface runoff as

176   described previously. We calculated the mean concentration of *E. coli* in surface runoff by weighing the

177   *E. coli* concentration exported from each land use by the annual areal percentage of each land use ([*E.*

178   *coli*]$_{OF-TOT}$). We also measured the *E. coli* concentration in water samples taken from three piezometers

179   (Ribolzi et al., 2018) and calculated the mean concentration of *E. coli* in groundwater ([*E. coli*]$_{GW-TOT}$).

180   ### 2.6. Electrical conductivity-based hydrograph separation

181   We used a tracer-based approach to separate storm hydrographs into 'event water' and 'pre-event

182   water'. This approach relies on a simple mixing model with two end-members and EC as a tracer. It is of

183   relatively low cost compared to e.g. isotopic tracers and was successfully tested in the study catchment

184   (Ribolzi et al., 2018). Based on previous field observations and measurements performed in the same

185   study catchment (Patin et al., 2012; Ribolzi et al., 2011; Vigiak et al., 2008), the two end-members of the

186   model (i.e. overland flow EC end-member in event water, and groundwater EC end-member in pre-event

187   water) can be interpreted in terms of hydrological processes. Event water mainly includes infiltration

188   excess that produces overland flow along hillslopes. Pre-event water relates to groundwater that feeds

189   the stream during the storm event, plus the water in the stream channel prior to the storm event, which

190   is also related to groundwater outflows. As suggested by Collins and Neal (1998), we verified the linearity

191   between EC and the concentration of a conservative tracer to control the relevance of the EC-based

192   approach in our context (Ribolzi et al., 2018). The mixing model applied to individual samples is

193   described by the following equations:

$$Q = Q_{OF} + Q_{GW} \qquad\qquad\qquad\qquad \text{Eq. 1}$$

$$Q \times EC = Q_{OF} \times EC_{OF} + Q_{GW} \times EC_{GW} \qquad\qquad \text{Eq. 2}$$

194   where Q is the instantaneous stream water discharge at the catchment outlet (L s^{-1}), Q$_{OF}$ is the

195   instantaneous discharge of overland flow, i.e., event water or surface runoff (L s^{-1}), Q$_{GW}$ is the

196   instantaneous discharge of groundwater, i.e., pre-event water or sub-surface flow (L s^{-1}), EC is the

197   instantaneous electrical conductivity measured in the stream (μS cm^{-1}), EC_{OF} is the electrical conductivity

198   in overland flow (overland flow EC end-member; μS cm^{-1}), approximated from electrical conductivity

199   measurements in samples of overland flow collected at the soil surface on hillslopes draining to the

200   stream, and EC_{GW} is the electrical conductivity in groundwater (groundwater EC end-member; μS cm^{-1}),

201   approximated from the stream electrical conductivity at the beginning of the flood event, since

202   groundwater is the only supply of water to the stream during inter-storm flow periods (Ribolzi et al.,

203   2005). For each individual sample, we calculated the relative contributions of Q_{OF} and of Q_{GW} to Q based

204   on Eq. 2, namely Q_{OF}% and of Q_{GW}% (in %).

205   We assessed the uncertainty in estimating the contributions of overland flow and groundwater flow to

206   the total stream flow using the formulation of Genereux (1998), which assigns an uncertainty specific to

207   each term in Eqs. 1 and 2. The accuracy of Q is considered to be within ±10% of the measured value,

208   while the uncertainty of EC is approximately ±5% (Ribolzi et al., 2018). The uncertainties of both EC_{OF} and

209   EC_{GW} are estimated from the coefficients of variation (CV) of overland flow and groundwater samples,

210   respectively.

2.7. Flood-event variables

212   For each flood event, the mean concentration of *E. coli* ([*E. coli*]$_{mean}$) is equivalent to the average of the

213   instantaneous *E. coli* concentrations ([*E. coli*]) measured during the event, weighted by the

214   corresponding measurements of instantaneous discharge. We considered 13 candidate explanatory

215   variables to predict [*E. coli*]$_{mean}$:

216   -   Rainfall duration (R_D, in min), total rainfall (R_{TOT}, in mm), maximum rainfall intensity (RI_{MAX}, in mm

217   h^{-1});

218   -   Antecedent Precipitation Index (API, in mm), as a proxy of soil moisture conditions, calculated as

219          $API_n = (API_{n-1} + P_{n-1}) \times e^{-\alpha \times t}$ where API_{n-1} is the antecedent precipitation index prior to

220   rain event n-1 (mm), P_{n-1} is the rainfall precipitated during rain event n-1 (mm), α is the

221   calibration coefficient usually set at 0.5 (day^{-1}), and t is the duration between P_n and P_{n-1} (day)

222   (Descroix et al., 2002);

223   -   Peak discharge during flood event (Q_{MAX}, in L s^{-1}), total volume of stream water during flood

224   event (Q_{TOT}, in m^3), total volume of surface runoff, i.e. overland flow, during flood event (Q_{OF-TOT},

225   in m^3) and its contribution to Q_{TOT} (Q_{OF-TOT}%, in %), and volume of sub-surface flow during flood

226   event (Q_{GW-TOT}, in m^3) and its contribution to Q_{TOT} (Q_{GW-TOT}%, in %);

227   -   Flow coefficient of the flood event (K_E, no dimension), calculated as the ratio between Q_{TOT} and

228   R_{TOT};

229   -   Flood-event mean concentration of total suspended sediments concentration ([TSS]$_{mean}$, in g L^{-1}),

230   calculated by weighting [TSS] by the discharge, and flood-event mean turbidity (Turbidity$_{mean}$, in

231   NTU), calculated by weighting Turbidity by time.

2.8. Hysteresis

233 Combined with EC-based hydrograph separation, the analysis of rotational direction, curvature, and

234 trend of hysteresis relationships can be used to interpret the relative contributions from surface water

235 and groundwater, and analyte sources (Holz, 2010; Long et al., 2017). Here, we analyzed hysteresis

236 patterns of EC, Turbidity, [TSS] and [*E. coli*] against discharge; [TSS], Turbidity and [*E. coli*] against Q_{OF};

237 Turbidity and [*E. coli*] against [TSS]; and [*E. coli*] against Turbidity. For each flood, we considered straight

238 relationships when the p-value of the Pearson correlation was below 0.001. The threshold was

239 voluntarily chosen very demanding to distinguish straight relationships from other hysteretic patterns.

240   2.9. Statistical analysis

241 We calculated correlations and regressions to identify explanatory variables predicting [*E. coli*] and [*E.*

242 *coli*]$_{mean}$. Statistics were calculated with R statistical package version 3.4.3 (correlations), Minitab 18.1

243 (stepwise regression), and XLSTAT 20.1.1 (partial least square regression). An explanatory variable was

244 considered to be statistically significantly different from zero when its p-value, derived from Student's t-

245 test, was lower than 0.05.

246   2.9.1.   Modelling instantaneous *E. coli* concentration [*E. coli*]

247 We first calculated Pearson correlations between [*E. coli*] and the eight hydrological variables measured

248 or calculated for each sample (EC, Q, Q_{OF}, Q_{GW}, Q_{OF}%, Q_{GW}%, [TSS], and Turbidity). In addition, to select

249 the best set of explanatory variables predicting [*E. coli*], we derived linear regressions from the 'step-

250 wise regression' selection algorithm. This selection intended to maximize the prediction R² (R^2_{pred})

251 calculated by leave-one-out cross-validations. This performance criterion reflects the ability of the model

252 to predict observations that were not used in the model calibration. Its maximization leads to greater

253 parsimony in the number of explanatory variables (Helsel and Hirsch, 2002). We verified the required

254 homoscedasticity of the model's residuals by visual inspection. Multi-collinearity among the selected

255 explanatory variables was avoided by ensuring that the Variance Inflation Factor (VIF) never exceeded

256 the value of 8 (Helsel and Hirsch, 2002). We didn't mix instantaneous measurements with flood-event

257 variables or with variables assessed annually (Annual crop, Teak+Crop, Teak, and Fallow) or monthly (*E.*

258 *coli* input).

259   2.9.2.   Modelling mean concentration of *E. coli* per flood event [*E. coli*]$_{mean}$

260 We first calculated Pearson correlations between [*E. coli*]$_{mean}$ and the thirteen hydro-meteorological

261 variables measured or calculated for each flood event (Table 1) and the five land-use related variables

262 (Annual crop, Teak+Crop, Teak, Fallow, and *E. coli* input). In addition, we used Partial Least Square (PLS)

263   regression to detect dependencies between variables. PLS is able to handle datasets with a number of

264   variables higher than the number of observations. It is also poorly sensitive to multi-collinearity, and

265   handles missing data by imputation. The importance of each projected variable is estimated by the

266   Variable Importance in the Projection (VIP). We discarded the variables for which VIP values were below

267   1 (Ribolzi et al., 2016b; Wold, 1995).

268   2.10.   Mixing model of flood-event mean concentration of *E. coli*

269   We applied a simple mixing model with two end-members to predict [*E. coli*]$_{mean}$ and to separate the

270   contributions of both 'event water' and 'pre-event water' to the in-stream *E. coli* concentrations. Here

271   the two end-members of the model are *E. coli* concentration in event water (overland flow *E. coli* end-

272   member or [*E. coli*]$_{OF-TOT}$) and *E. coli* concentration in pre-event water (groundwater *E. coli* end-member

273   or [*E. coli*]$_{GW-TOT}$). The mixing model applied to flood-event mean variables is described by the following

274   equations:

$$Q_{TOT} = Q_{OF-TOT} + Q_{GW-TOT}$$ Eq. 3

$$Q_{TOT} \times [E.coli]_{mean} = Q_{OF-TOT} \times [E.coli]_{OF-TOT} + Q_{GW-TOT} \times [E.coli]_{GW-TOT}$$ Eq. 4

275   where Q_{TOT} is the total volume of stream water during flood event (m^3), Q_{OF-TOT} is the total volume of

276   surface runoff, or overland flow, during flood event (m^3), Q_{GW-TOT} is the total volume of sub-surface flow,

277   or groundwater flow, during flood event (m^3), [*E. coli*]$_{mean}$ is the flood-event mean concentration of *E. coli*

278   (MPN 100 mL^{-1}), [*E. coli*]$_{OF-TOT}$ is the mean concentration of *E. coli* exported in overland flow (MPN 100

279   mL^{-1}), calculated from *E. coli* concentration measured in samples of overland flow collected at the soil

280   surface on hillslopes draining to the stream, and [*E. coli*]$_{GW-TOT}$ is the mean concentration of *E. coli* in

281   groundwater (MPN 100 mL^{-1}), calculated from *E. coli* concentration measured in groundwater. This

282   approach was shown to yield a comparable or even higher performance when predicting in-stream

283   pathogen concentrations compared with more complex fate and transport models (Chin, 2011). We

284   applied the mixing model to the twelve flood events and compared its performance with the

285   performance of the PLS model. For each flood event, we calculated the relative contributions of [*E.*

286   *coli*]$_{OF-TOT}$ and of [*E. coli*]$_{GW-TOT}$ to [*E. coli*]$_{mean}$ based on Eq. 4, namely [*E. coli*]$_{OF-TOT}$% and of [*E. coli*]$_{GW-TOT}$%

287   (in %).

288   3. Results

289   3.1. *E. coli* dynamics during flood events and among flood events

290   The areal percentage of land use evolved from 2011 to 2015 (Fig. SI1): annual crop decreased from 28%

291   to 4% of the catchment area, and teak and annual crop decreased from 12% to 0%, while teak increased

292   from 18% to 36%, and fallow increased from 29% to 46%. Areal percentage of forest was constant at 8%.

293   The *E. coli* input into the catchment decreased from a monthly average of $2x10^{15}$ in 2011 to a monthly

294   average of $3x10^{14}$ in 2015 (Fig. SI2). Over the 2011-2015 period, the cumulated *E. coli* input for swine and

295   poultry accounted for 0.01-0.38 % of the total *E. coli* input.

296   In the meantime, a total of 294 discharge peaks were recorded between January 1, 2011, and December

297   31, 2015 (Fig. 2), in response to a range of rainfall events (Fig. SI3, see interquartile ranges): 50 % of R_{TOT}

298   ranged between 7 and 22 mm, 50 % of RI_{MAX} ranged between 24 and 60 mm h^{-1}, and 50 % of R_D ranged

299   between 49 and 235 min. Q ranged from 0 to 1 807.6 L s^{-1} (30 L s^{-1} ha^{-1}), with a mean Q of 33.3 L s^{-1}.

300   We monitored twelve flood events (A to L) for stream water quality. Datasets for each of the twelve

301   flood events are complete except EC measurements lacking for event A and Turbidity measurements

302   lacking for event G, due to measurement devices' breakdown. A total of 99 stream water samples was

303   collected: [TSS] ranged from 0.02 to 25.7 g L^{-1} while Turbidity ranged from 191.8 to 13 480 NTU (Fig. 3).

304   *E. coli* were detected in all samples and [*E. coli*] ranged between 160 and 74 000 MPN 100 mL^{-1} (Fig. 3).

305   For the twelve flood events, rainfall was followed by an increase of Q, Turbidity, [TSS] and [*E. coli*] (Fig.

306   3). However, the peaks of Q, Turbidity, [TSS] and [*E. coli*] were often asynchronous (full description is

307   given in the supplementary information). Hysteresis loops showed complex patterns mixing straight

308   lines, simple clockwise or anti-clockwise loops, figures-of-eight or multiple hysteresis loops (summary is

309   presented in Table SI1, full description is given in the supplementary information, including Figs. SI4-SI7).

310   The uncertainty bands enclosing Q_{OF} and Q_{GW} in Fig. 3 show that the hydrograph could be clearly

311   separated for each flood event. Flood event C was the only event where the stream flow was virtually

312   100% groundwater flow. Excluding flood event C, Q_{OF-TOT}% ranged between 17 and 80% (Fig. 4a). The

313   average Q_{OF-TOT}% was 41% (CV=0.59).

314   The twelve flood events corresponded to a range of storm characteristics in terms of R_{TOT}, RI_{MAX} and R_D

315   (Fig. SI3, Fig. 2). Q_{MAX} ranged from 31.7 to 967.9 L s^{-1} (Table 1, Fig. 3). Three flood events occurred after

316   dry periods (events B, G, and I: API<10), whereas others occurred shortly after a previous flood event

317   (events D, E, and J: API>30) or later (events A, C, F, H, K, and L: 10<API<20) (Table 1). [*E. coli*]$_{mean}$ ranged

318   from 1 125 and 27 375 MPN 100 mL^{-1}.

319   Mean EC_{OF} was 55 µS cm^{-1} (CV=0.7) over the 2011-2015 period (65 surface runoff water samples). Mean

320   EC_{GW} was 256 µS cm^{-1} (CV=0.42) among the twelve flood events. [*E. coli*]$_{OF-TOT}$ was 24 880, 27 292, 27 441,

321   26 987, and 26 935 MPN 100 mL^{-1} in 2011, 2012, 2013, 2014, and 2015, respectively (26 surface runoff

322   water samples). [*E. coli*]$_{GW-TOT}$ was 277 MPN 100 mL^{-1} (6 groundwater samples).

323   ## 3.2. Statistical analysis

324   ### 3.2.1. Modelling instantaneous *E. coli* concentration [*E. coli*]

325   Considering all water samples collected during the flood events (Fig. SI8), [*E. coli*] was positively

326   correlated to Q (r=0.54, p<0.001), Q_{OF} (r=0.56, p<0.001), Q_{OF}% (r=0.51, p<0.001), [TSS] (r=0.43, p<0.001),

327   and Turbidity (r=0.43, p<0.001), and was negatively correlated to EC (r=-0.31, p=0.003), and to Q_{GW}% (r=-

328   0.51, p<0.001). Turbidity was positively correlated to [TSS] (r=0.82, p<0.001).

329   From the stepwise regression, [*E. coli*] was best predicted by [TSS] and Q_{OF} (Eq. 5):

$$[E.coli] = 4995 + 689 \cdot [TSS] + 41.49 \cdot Q \qquad\qquad \text{Eq. 5}$$

330   T-values and p-values of the coefficients are given in Table SI2. The R² of the model is 35.3 % and the

331   R^2_{pred} is 24.42 %.

3.2.2. Modelling mean concentration of *E. coli* per flood event [*E. coli*]$_{mean}$

333   [*E. coli*]$_{mean}$ was positively correlated to Q_{MAX} (r=0.71, p=0.009), Q_{TOT} (r=0.59, p=0.042), Q_{OF-TOT} (r=0.72,

334   p=0.012), and Q_{OF-TOT}% (r=0.93, p<0.001), and was negatively correlated to Q_{GW-TOT}% (r=-0.93, p<0.001)

335   (Fig. SI9).

336   From the above, we found that Q_{OF-TOT}% was the variable the most positively correlated to [*E. coli*]$_{mean}$.

337   The linear model is:

$$[E.coli]_{mean} = 332 \cdot Q_{OF-TOT}\% - 3\,749 \qquad \text{Eq. 6}$$

338   The R² between predicted and observed [*E. coli*]$_{mean}$ was 0.87 while the Nash-Sutcliffe efficiency (NSE)

339   was 0.84 (Fig. 5a). Excluding event C that was driven by groundwater flow only (and for which the linear

340   model predicted a negative value), [*E. coli*]$_{mean}$ predicted by the linear model ranged from 1 981 to 22

341   825 MPN 100 mL^{-1}.

342   These latter trends are confirmed by the PLS regression (Fig. 6a), which shows that Axis 1 mostly explains

343   the variables Q_{OF-TOT}% (r=0.863), Q_{GW-TOT}% (r=-0.863), Q_{MAX} (r= 0.859), and Q_{OF-TOT} (r=0.815) whereas Axis 2

344   mostly explains the variable RI_{MAX} (r=0.563). Hence, Axis 1 corresponds to variables that are strongly

345   related to stream water whereas Axis 2 corresponds to variables describing rainfall and soil moisture

346   conditions. Accordingly, the twelve flood events were scattered along the two axes, with the flood

347   events of highest [*E. coli*]$_{mean}$ in the right panel (Fig. 6b). The variables with VIP values above 1 were Q_{OF-}

348    $_{TOT}$%, Q_{GW-TOT}%, Q_{MAX}, Q_{OF-TOT}, and Q_{TOT} when considering one component and Q_{OF-TOT}%, Q_{GW-TOT}%,

349   [TSS]$_{mean}$, Q_{MAX}, and Q_{OF-TOT} when considering two components (Fig. 6c; Table SI3). The statistical model

350   given by the PLS is given in Table SI3. The R² between predicted and observed [*E. coli*]$_{mean}$ was 0.83 while

351   the NSE was 0.78 (Fig. 5b). Excluding event C that was driven by groundwater flow only (and for which

352   the PLS model predicted a negative value), $[E.\ coli]_{mean}$ predicted by the PLS model ranged from 1 067 to

353   23 237 MPN 100 mL^{-1}.

354    $[E.\ coli]_{mean}$ predicted by the mixing model ranged from 277 to 21 572 MPN 100 mL^{-1}. The R² between

355   predicted and observed $[E.\ coli]_{mean}$ was 0.86 while the NSE was 0.65 (Fig. 5c). Flood event C was the only

356   event where the percentage of *E. coli* was 100% from groundwater flow. Excluding flood event C, [*E.*

357   *coli*]$_{OF-TOT}$% ranged from 95 to virtually 100% (Fig. 4b). The average $[E.\ coli]_{OF-TOT}$% was 89% (CV=0.33).

358

359

360   4.   Discussion

361   4.1. High *E. coli* concentration pulses match high overland flow pulses

362   The analysis of the twelve monitored flood events (Table 1) shows that [*E. coli*]$_{mean}$ was high regardless of

363   the flood event characteristics: [*E. coli*]$_{mean}$ ranged between 1 125 and 27 375 MPN 100 mL^{-1}. The order of

364   magnitude of the maximum [*E. coli*] is about 10^5 MPN 100 mL^{-1}. All these values exceed the 1 000

365   MPN 100 mL^{-1} threshold provided by e.g. the European Directive 2006/7/EC for bathing water quality.

366   Although rainfall is known to reactivate hydrological connectivity (Bracken et al., 2013), rainfall

367   characteristics such as R_{T0T}, RI_{MAX}, and R_D, did not appear as strong explanatory variables of [*E. coli*]$_{mean}$

368   (Fig. 6 and Fig. SI9). Variations in [*E. coli*] and [*E. coli*]$_{mean}$ between flood events may be explained by

369   rainfall spatial distribution and the timing between rainfall events: the rainfall distribution will determine

370   which areas draining animal and human manure are activated, whereas the timing between events may

371   indicate which catchment microbial stocks have accumulated to high levels (McKergow and Davies-

372   Colley, 2010). In Houay Pano catchment, variations in concentration between flood events may also be

373   explained by *E. coli* input distribution at the soil surface, as the land use is mixed (Fig. SI1). Indeed, based

374   on this twelve-event dataset and hysteresis analysis, we could not find any clear, consistent trend at the

375   outlet of the Houay Pano catchment (Table SI1) and we thus could not identify any primary bacteria

376   source.

377   The land use change in Houay Pano catchment was rapid and led to the simultaneous increase of teak

378   tree plantations and of fallow areas (Ribolzi et al., 2017). Previous plot- and catchment-scale results

379   showed higher surface runoff and suspended matter export when teak tree plantations increased

380   (Lacombe et al., 2018; Mügler et al., 2019; Ribolzi et al., 2017; Song et al., 2020), suggesting that higher

381   numbers of *E. coli* could be transferred to the river. However, land use characteristics such as land use

382   variables (Annual crop, Teak+Crop, Teak, Fallow, and *E. coli* input) did not appear as strong explanatory

383　variables of [*E. coli*]$_{mean}$ (Fig. 6 and Fig. SI10). Growing teak trees and fallow requires less people in the

384　field compared to annual crops. Since field workers practice open defecation, less workers imply lower

385　input of *E. coli* into the catchment. The contribution of domestic animals to the overall *E. coli* input being

386　only 0.01-0.38 % of the total *E. coli* input, the consequence of the extension of teak tree plantation and

387　of fallow in Houay Pano from 2011 to 2015 (Fig. SI1) is the overall decrease of the *E. coli* input into the

388　catchment over the same period (Fig. SI2).

389　The highest [*E. coli*]$_{mean}$ was often associated to flood events with highest Q_{MAX} (events J and L) and

390　dominant surface runoff (Q_{OF-TOT}%>50: events D, and I-L), confirming the role of surface runoff, and

391　subsequent soil surface erosion, in *E. coli* transfers to the stream (Causse et al., 2015) (Table 1, Fig. 6).

392　For flood events where sub-surface flow was dominating (Q_{OF-TOT}%<50: events B, C, and E-H), [*E. coli*]$_{mean}$

393　was in general lower, although exceeding 1 000 MPN 100 mL^{-1}. High *E. coli* concentrations even when

394　sub-surface flow was dominating suggest that streambanks and the streambed may release stored *E. coli*

395　(Chu et al., 2011; Park et al., 2017; Stocker et al., 2018) since sediment deposited at the bottom of the

396　stream may act as an *E. coli* reservoir (Pachepsky et al., 2017; Rochelle-Newall et al., 2015; Smith et al.,

397　2008). In fact, the concentration of *E. coli* in Houay Pano streambed sediment is about 40 000 MPN g^{-1}

398　(Ribolzi et al., 2016a), but we cannot exclude that *E. coli* is simultaneously transferred from the hillslope

399　with surface runoff, if hillslope soil surface is highly contaminated. We also found both clockwise and

400　anti-clockwise [*E. coli*]-[TSS] and [*E. coli*]-Turbidity hysteresis loops, and in some cases figure-of-eight

401　patterns (Table SI1, Fig. SI6 and Fig. SI7). This further suggests that the erosion of bacteria stores is not

402　strictly driven by soil erosion, but also by in-stream sediment resuspension (Evrard et al., 2016; Gourdin

403　et al., 2015; Huon et al., 2017). In parallel, possibly less *E. coli*-contaminated sub-surface flow, or return

404　flow, may dilute in the stream the *E. coli* concentration originating from surface runoff and thus mitigate

405　the in-stream microbial contamination.

4.2. Predictive models of *E. coli* concentration: performances and usefulness

To our knowledge, few studies have reported predictive models using independent variables to explain *E. coli* concentration and, to the best of our knowledge, they were all developed in temperate areas (Chen and Chang, 2014; Hathaway et al., 2010). The models suggested by Chen and Chang (2014) included antecedent precipitation, stream temperature, and TSS concentration, and gave an R^2 of 0.27-0.61 depending on the season and the catchment. The model suggested by Hathaway et al. (2010) included temperature, rainfall, and humidity, and had an R^2 of 0.7462. The variety of explanatory variables among models reflects the variety of driving processes driving *E. coli* fate and transport among catchments.

4.2.1. Modelling instantaneous *E. coli* concentration [*E. coli*]

[*E. coli*] was equally correlated to both [TSS] and Turbidity (r=0.43, p<0.001; Fig. SI8) while Turbidity was correlated with [TSS] (r=0.82, p<0.001, Fig. SI8). The strong correlation between Turbidity and [TSS] is in line with the results obtained in other studies in tropical areas, such as Ziegler et al. (2014) for rivers in Thailand and Robert et al. (2017) in West African lakes and ponds. The relationships between [TSS] and [*E. coli*] and between Turbidity and [*E. coli*] are qualified by hysteretic trends (Figs. SI6 and SI7, respectively) during flood events. Notably, little hysteresis is observed between [TSS] and Turbidity (Fig. SI6). Hysteretic trends may illustrate the uncertainty when predicting *E. coli* by a proxy such as turbidity: sources of sediments may not exactly coincide with sources of *E. coli*. For example, these relationships may not apply in large mixed-land use catchments, because of the multiple, geographically separated, *E. coli* and turbidity sources. This may limit the usefulness of using turbidity as a proxy of *E. coli* near the catchment outlet (McKergow and Davies-Colley, 2010). Another explanation of the hysteresis is the nature and the properties of the suspended sediments, that may change during the flood event: bacteria may be less prone to attach to sand-rich suspended particles (Oliver et al., 2007). Similarly, hysteresis in Turbidity-[TSS] relationships may be explained by changing reflectance properties of the suspended

430   sediments depending on particle size, shape, mineralogy, aggregation/flocculation, dissolved light-

431   absorbing matter and bubbles, because of the spatial heterogeneity of rainfall and suspended sediment

432   sources at the catchment scale (Navratil et al., 2011; Ziegler et al., 2014). A last uncertainty source in the

433   relationships between [*E. coli*], [TSS], and Turbidity, is the possible exhaustion of the *E. coli* stock within

434   the catchment after a succession of flood events.

435   From the step-wise regression analysis, the predictive model for [*E. coli*] includes [TSS] and Q_{OF} as

436   explanatory variables (Eq. 5). The two explanatory variables reflect the two processes driving *E. coli*

437   transport within the catchment: Q_{OF} reflects the mobilization of *E. coli* with relative contributions of

438   surface and sub-surface flows along the flood event, whereas [TSS] reflects the attachment of *E. coli* to

439   soil particles and/or streambed resuspended sediments (Garcia-Armisen and Servais, 2009; Nguyen et

440   al., 2016). Overall, higher *E. coli* concentration is related to higher surface runoff and higher suspended

441   matter in the stream flow. The value of the intercept term in Eq. 5 corresponds to *E. coli* concentration

442   during base flow (Boithias et al., 2016; Kim et al., 2018), i.e. when [TSS] and Q_{OF} tend to zero because

443   there is no surface runoff during inter-storm periods, in other words when groundwater is the only

444   supply to stream flow and EC tends to EC_{GW}.

445   The two variables best predicting [*E. coli*], namely [TSS] and Q_{OF}, can be assessed with proxies. [TSS]

446   could be interchanged with Turbidity, since [TSS] and Turbidity are correlated, as discussed above.

447   Similarly, EC appears strongly related to Q_{OF} (and Q) by a hyperbolic function (Fig. SI8). Using EC as a

448   proxy of Q has already been proposed in Alpine headwaters (Cano-Paoli et al., 2019). Both of these

449   proxies can be monitored *in situ* at high frequencies.

450   4.2.2.   Modelling mean concentration of *E. coli* per flood event [*E. coli*]$_{mean}$

451   The PLS regression analysis (Table SI3) confirmed the analysis of the correlation matrix (Fig. SI9): Q_{OF-TOT}%

452   and Q_{GW-TOT}% were the best predictors of [*E. coli*]$_{mean}$ (r= 0.93 and -0.93, respectively). Land uses that

453   favor higher Q_{OF-TOT}% or lower Q_{GW-TOT}%, such as erosion-prone teak trees plantations (Lacombe et al.,

454   2016; Ribolzi et al., 2017), or more intense rainfall events, will lead to higher in-stream concentrations of

455   *E. coli* (Fig. 6a and Fig. SI10) and thus higher fecal contamination risk. Hence, a model based on Q_{OF-TOT}%

456   or Q_{GW-TOT}% appears relevant to predict $[E.\ coli]_{mean}$. Such a basic tool may help local and national

457   stakeholders to assess the fecal contamination risk by testing global change scenarios in target

458   catchments.

459   In this study, the mixing model of $[E.\ coli]_{mean}$ based on Q_{OF-TOT}% and Q_{GW-TOT}% had a R^2 of 0.86 and a NSE

460   of 0.65. The NSE value is lower than the NSE values' range reported by Chin (2011) in six nested

461   catchments in Georgia, United-States. However, in our study the values of both overland flow and

462   groundwater end-members were measured in the field, conversely to Chin (2011) who numerically

463   optimized the values of the two end-members. The performance of the mixing model is lower in terms of

464   NSE than those of the PLS and the linear models (NSE = 0.78 and 0.84, respectively). However, the PLS

465   model is difficult to implement because of the large number of variables it implies, and both the linear

466   and the PLS models are constrained by their validity domains.

467   Within a catchment, the sources of *E. coli* are the *E. coli* transferred from hillslopes with surface runoff,

468   as discussed in section 4.1, and the resuspension from the streambed, whereas the sinks of *E. coli* are the

469   deposition of the bacterium on the streambed and its decay in the water column. Since rainfall events in

470   the Houay Pano catchment last 0.5-5 hours, considering a decay rate of 0.3-0.6 d^{-1} (Nguyen et al., 2016),

471   the removal of *E. coli* in the water column from bacteria population decay is negligible during a flood

472   event. Since the mixing model is able to accurately predict the flood-event mean concentration of *E. coli*

473   at the catchment outlet, the deposition of *E. coli* on the streambed is either negligible or compensated

474   by the resuspension. The percentage of *E. coli* resuspended from streambed during a flood is about 11%

475   (Ribolzi et al., 2016a), which implies that the compensated *E. coli* deposition, e.g. in small wetlands along

476   the main stream, is about 11% as well. Finally, since the possible sources and sinks of *E. coli* are negligible

477   compared to the bacterium transport processes during flood events, the approximation of the simple

478   model that only considers two end-members, namely the *E. coli* concentration in both surface runoff and

479   groundwater, is acceptable.

480   Hence, we could calculate the relative contributions of surface runoff and of sub-surface flow to the in-

481   stream *E. coli* contamination. Excluding flood event C that was driven by groundwater flow, more than

482   95% of $[E.\ coli]_{mean}$ resulted from overland flow, even for flood events where the percentage of overland

483   flow was small (<20%, events E and G). The average contribution of overland flow to the flood-event

484   mean concentration of *E. coli* was 89%, while the average contribution of overland flow to the flood-

485   event mean stream flow was 41% (Fig. 4). In other words, the contribution of groundwater to the in-

486   stream *E. coli* contamination was low during flood events, even though the contribution of groundwater

487   to stream water flow was greater than that of overland flow, i.e. when base flow index (BFI) was over

488   0.5. In comparison, with similar BFI values, Chin (2011) reported bacteria loads from surface runoff in the

489   range of 80–90%, with the remainder mostly originating from base flow, and negligible background loads

490   from the catchment.

491

492 5. Conclusion

493 To our knowledge, few papers have reported the statistical relationships between *E. coli* and its

494 environmental drivers (meteorological, hydrological, and land use variables) and the present study is the

495 first one to investigate *E. coli* dynamics during flood events in a tropical humid catchment. We conclude

496 that:

497 - Regardless of the contribution of sub-surface flow to the flood, in-stream *E. coli* concentration is

498 high, suggesting that the streambed *E. coli* store is high. However, highest concentrations of *E.*

499 *coli* are measured for the flood events that are driven by surface runoff, suggesting that surface

500 runoff, and consequently soil erosion, are the primary drivers of in-stream *E. coli* contamination;

501 - The three predictive models (linear model, partial least square model, and mixing model) show

502 that the percentage of surface runoff in stream flow is the best predictor of the flood event

503 mean concentration of *E. coli*;

504 - A simple mixing model based on the relative contributions of both overland flow and

505 groundwater, and on the *E. coli* concentration in both overland flow and groundwater, is reliable

506 to predict in-stream flood-event mean *E. coli* concentration (NSE=0.65). On average, 89% of the

507 in-stream concentration of *E. coli* is supplied by surface runoff, while the overall contribution of

508 surface runoff to the stream flow is 41%.

509 - Stream flow turbidity and *E. coli* concentration are positively correlated, but turbidity is not a

510 strong predictor of *E. coli* concentration during flood events;

511 Predictive models based on turbidity and electrical conductivity may be used to provide real-time

512 estimates of in-stream *E. coli* concentration, whereas a mixing model may provide flood-event mean

513 information. Such simple models may help to assess the impact of global change on in-stream *E. coli*

514 contamination. They could thus be used to assess the risk of water borne diseases such as diarrhea, in

515 rural areas where mammals, including humans, practice open defecation, and to design early warning

25

516 systems. Applied over long periods of time, the models might be used to calculate *E. coli* input-output

517 load balances. Such basic modelling studies would thus help to assess the long-term impact of land-use

518 change on the microbial quality of surface water.

519 Future work is required to better understand the pathways of FIB at catchment scale. For example, there

520 is a need to characterize the interactions between ground and surface waters, and the role of the

521 hyporheic zone, as sources of contaminant. Furthermore, the partition between free and particle-

522 attached *E. coli* should be quantified to better understand and predict the probability that bacteria is

523 deposited on the streambed during the flood recession stage and re-suspended in the water column

524 during the next flood rising stage. These findings are of primary importance to build adequate

525 catchment-scale models to accurately simulate *E. coli* fate and transport, and thus better assess fecal

526 contamination risk in a global changing context.

527

536

537

References

Boithias, L., Auda, Y., Audry, S., et al., 2020. Dataset from the Multiscale TROPIcal CatchmentS critical zone observatory M-TROPICS II: land use, hydrology and sediment production monitoring in Houay Pano, northern Lao PDR. Hydrol. Process. Submitted.

Boithias, L., Choisy, M., Souliyaseng, N., Jourdren, M., Quet, F., Buisson, Y., Thammahacksa, C., Silvera, N., Latsachack, K., Sengtaheuanghoung, O., Pierret, A., Rochelle-Newall, E., Becerra, S., Ribolzi, O., 2016. Hydrological regime and water shortage as drivers of the seasonal incidence of diarrheal diseases in a tropical montane environment. PLoS Negl. Trop. Dis. 10, e0005195. https://doi.org/10.1371/journal.pntd.0005195

Bracken, L.J., Wainwright, J., Ali, G.A., Tetzlaff, D., Smith, M.W., Reaney, S.M., Roy, A.G., 2013. Concepts of hydrological connectivity: Research approaches, pathways and future agendas. Earth-Sci. Rev. 119, 17–34. https://doi.org/10.1016/j.earscirev.2013.02.001

Cano-Paoli, K., Chiogna, G., Bellin, A., 2019. Convenient use of electrical conductivity measurements to investigate hydrological processes in Alpine headwaters. Sci. Total Environ. 685, 37–49. https://doi.org/10.1016/j.scitotenv.2019.05.166

Causse, J., Billen, G., Garnier, J., Henri-des-Tureaux, T., Olasa, X., Thammahacksa, C., Latsachak, K.O., Soulileuth, B., Sengtaheuanghoung, O., Rochelle-Newall, E., Ribolzi, O., 2015. Field and modelling studies of Escherichia coli loads in tropical streams of montane agro-ecosystems. J. Hydro-Environ. Res. 9, 496–507. https://doi.org/10.1016/j.jher.2015.03.003

Chen, H.J., Chang, H., 2014. Response of discharge, TSS, and E. coli to rainfall events in urban, suburban, and rural watersheds. Env. Sci Process. Impacts 16, 2313–2324. https://doi.org/10.1039/C4EM00327F

Chin, D.A., 2011. Quantifying pathogen sources in streams by hydrograph separation. J. Environ. Eng. 137, 770–781.

Cho, K.H., Han, D., Park, Y., Lee, S.W., Cha, S.M., Kang, J.-H., Kim, J.H., 2010. Evaluation of the relationship between two different methods for enumeration fecal indicator bacteria: Colony-forming unit and most probable number. J. Environ. Sci. 22, 846–850. https://doi.org/10.1016/S1001-0742(09)60187-X

Cho, K.H., Pachepsky, Y.A., Oliver, D.M., Muirhead, R.W., Park, Y., Quilliam, R.S., Shelton, D.R., 2016. Modeling fate and transport of fecally-derived microorganisms at the watershed scale: State of the science and future opportunities. Water Res. 100, 38–56. https://doi.org/10.1016/j.watres.2016.04.064

Chu, Y., Salles, C., Tournoud, M.-G., Got, P., Troussellier, M., Rodier, C., Caro, A., 2011. Faecal bacterial loads during flood events in Northwestern Mediterranean coastal rivers. J. Hydrol. 405, 501–511. https://doi.org/10.1016/j.jhydrol.2011.05.047

Chuah, C.J., Ziegler, A.D., 2018. Temporal Variability of Faecal Contamination from On-Site Sanitation Systems in the Groundwater of Northern Thailand. Environ. Manage. https://doi.org/10.1007/s00267-018-1016-7

Collins, R.U., Neal, C., 1998. The hydrochemical impacts of terraced agriculture, Nepal. Sci. Total Environ. 212. https://doi.org/10.1016/S0048-9697(97)00342-2

Descroix, L., Nouvelot, J.-F., Vauclin, M., 2002. Evaluation of an antecedent precipitation index to model runoff yield in the western Sierra Madre (North-west Mexico). J. Hydrol. 263, 114–130. https://doi.org/10.1016/S0022-1694(02)00047-1

Evrard, O., Laceby, J.P., Huon, S., Lefèvre, I., Sengtaheuanghoung, O., Ribolzi, O., 2016. Combining multiple fallout radionuclides (137Cs, 7Be, 210Pbxs) to investigate temporal sediment source dynamics in tropical, ephemeral riverine systems. J. Soils Sediments 16, 1130–1144. https://doi.org/10.1007/s11368-015-1316-y

585 Exley, J.L.R., Liseka, B., Cumming, O., Ensink, J.H.J., 2015. The Sanitation Ladder, What Constitutes an
586   Improved Form of Sanitation? Environ. Sci. Technol. 49, 1086–1094.
587   https://doi.org/10.1021/es503945x
588 Gaillardet, J., Braud, I., Hankard, F., Anquetin, S., Bour, O., Dorfliger, N., de Dreuzy, J.R., Galle, S., Galy, C.,
589   Gogo, S., Gourcy, L., Habets, F., Laggoun, F., Longuevergne, L., Le Borgne, T., Naaim-Bouvet, F.,
590   Nord, G., Simonneaux, V., Six, D., Tallec, T., Valentin, C., Abril, G., Allemand, P., Arènes, A., Arfib,
591   B., Arnaud, L., Arnaud, N., Arnaud, P., Audry, S., Comte, V.B., Batiot, C., Battais, A., Bellot, H.,
592   Bernard, E., Bertrand, C., Bessière, H., Binet, S., Bodin, J., Bodin, X., Boithias, L., Bouchez, J.,
593   Boudevillain, B., Moussa, I.B., Branger, F., Braun, J.J., Brunet, P., Caceres, B., Calmels, D.,
594   Cappelaere, B., Celle-Jeanton, H., Chabaux, F., Chalikakis, K., Champollion, C., Copard, Y., Cotel,
595   C., Davy, P., Deline, P., Delrieu, G., Demarty, J., Dessert, C., Dumont, M., Emblanch, C., Ezzahar, J.,
596   Estèves, M., Favier, V., Faucheux, M., Filizola, N., Flammarion, P., Floury, P., Fovet, O., Fournier,
597   M., Francez, A.J., Gandois, L., Gascuel, C., Gayer, E., Genthon, C., Gérard, M.F., Gilbert, D.,
598   Gouttevin, I., Grippa, M., Gruau, G., Jardani, A., Jeanneau, L., Join, J.L., Jourde, H., Karbou, F.,
599   Labat, D., Lagadeuc, Y., Lajeunesse, E., Lastennet, R., Lavado, W., Lawin, E., Lebel, T., Le
600   Bouteiller, C., Legout, C., Lejeune, Y., Le Meur, E., Le Moigne, N., Lions, J., Lucas, A., Malet, J.P.,
601   Marais-Sicre, C., Maréchal, J.C., Marlin, C., Martin, P., Martins, J., Martinez, J.M., Massei, N.,
602   Mauclerc, A., Mazzilli, N., Molénat, J., Moreira-Turcq, P., Mougin, E., Morin, S., Ngoupayou, J.N.,
603   Panthou, G., Peugeot, C., Picard, G., Pierret, M.C., Porel, G., Probst, A., Probst, J.L., Rabatel, A.,
604   Raclot, D., Ravanel, L., Rejiba, F., René, P., Ribolzi, O., Riotte, J., Rivière, A., Robain, H., Ruiz, L.,
605   Sanchez-Perez, J.M., Santini, W., Sauvage, S., Schoeneich, P., Seidel, J.L., Sekhar, M.,
606   Sengtaheuanghoung, O., Silvera, N., Steinmann, M., Soruco, A., Tallec, G., Thibert, E., Lao, D.V.,
607   Vincent, C., Viville, D., Wagnon, P., Zitouna, R., 2018. OZCAR: The French Network of Critical Zone
608   Observatories. Vadose Zone J. 17, 180067. https://doi.org/10.2136/vzj2018.04.0067
609 Garcia-Armisen, T., Servais, P., 2009. Partitioning and Fate of Particle-Associated E. coli in River Waters.
610   Water Environ. Res. 81, 21–28. https://doi.org/10.2175/106143008X304613
611 Genereux, D., 1998. Quantifying uncertainty in tracer-based hydrograph separations. Water Resour. Res.
612   34, 915–919. https://doi.org/10.1029/98WR00010
613 Gourdin, E., Huon, S., Evrard, O., Ribolzi, O., Bariac, T., Sengtaheuanghoung, O., Ayrault, S., 2015. Sources
614   and export of particle-borne organic matter during a monsoon flood in a catchment of northern
615   Laos. Biogeosciences 12, 1073–1089. https://doi.org/10.5194/bg-12-1073-2015
616 Hathaway, J.M., Hunt, W.F., Simmons, O.D., 2010. Statistical Evaluation of Factors Affecting Indicator
617   Bacteria in Urban Storm-Water Runoff. J. Environ. Eng. 136, 1360–1368.
618   https://doi.org/10.1061/(ASCE)EE.1943-7870.0000278
619 Helsel, D.R., Hirsch, R.M., 2002. Chapter A3: Statistical Methods in Water Resources, in: Techniques of
620   Water-Resources Investigations of the United States Geological Survey. Book 4, Hydrologic
621   Analysis and Interpretation.
622 Holz, G.K., 2010. Sources and processes of contaminant loss from an intensively grazed catchment
623   inferred from patterns in discharge and concentration of thirteen analytes using high intensity
624   sampling. J. Hydrol. 383, 194–208. https://doi.org/10.1016/j.jhydrol.2009.12.036
625 Huon, S., Evrard, O., Gourdin, E., Lefèvre, I., Bariac, T., Reyss, J.-L., Henry des Tureaux, T.,
626   Sengtaheuanghoung, O., Ayrault, S., Ribolzi, O., 2017. Suspended sediment source and
627   propagation during monsoon events across nested sub-catchments with contrasted land uses in
628   Laos. J. Hydrol. Reg. Stud. 9, 69–84. https://doi.org/10.1016/j.ejrh.2016.11.018
629 Kim, M., Boithias, L., Cho, K.H., Sengtaheuanghoung, O., Ribolzi, O., 2018. Modeling the Impact of Land
630   Use Change on Basin-scale Transfer of Fecal Indicator Bacteria: SWAT Model Performance. J.
631   Environ. Qual. 47, 1115–1122. https://doi.org/10.2134/jeq2017.11.0456

632   Kim, M., Boithias, L., Cho, K.H., Silvera, N., Thammahacksa, C., Latsachack, K., Rochelle-Newall, E.,
633   Sengtaheuanghoung, O., Pierret, A., Pachepsky, Y.A., Ribolzi, O., 2017. Hydrological modeling of
634   Fecal Indicator Bacteria in a tropical mountain catchment. Water Res. 119, 102–113.
635   https://doi.org/10.1016/j.watres.2017.04.038
636   Krometis, L.-A.H., Characklis, G.W., Simmons, O.D., Dilts, M.J., Likirdopulos, C.A., Sobsey, M.D., 2007.
637   Intra-storm variability in microbial partitioning and microbial loading rates. Water Res. 41, 506–
638   516. https://doi.org/10.1016/j.watres.2006.09.029
639   Lacombe, G., Ribolzi, O., de Rouw, A., Pierret, A., Latsachak, K., Silvera, N., Pham Dinh, R., Orange, D.,
640   Janeau, J.-L., Soulileuth, B., Robain, H., Taccoen, A., Sengphaathith, P., Mouche, E.,
641   Sengtaheuanghoung, O., Tran Duc, T., Valentin, C., 2016. Contradictory hydrological impacts of
642   afforestation in the humid tropics evidenced by long-term field monitoring and simulation
643   modelling. Hydrol. Earth Syst. Sci. 20, 2691–2704. https://doi.org/10.5194/hess-20-2691-2016
644   Lacombe, G., Valentin, C., Sounyafong, P., de Rouw, A., Soulileuth, B., Silvera, N., Pierret, A.,
645   Sengtaheuanghoung, O., Ribolzi, O., 2018. Linking crop structure, throughfall, soil surface
646   conditions, runoff and soil detachment: 10 land uses analyzed in Northern Laos. Sci. Total
647   Environ. 616–617, 1330–1338. https://doi.org/10.1016/j.scitotenv.2017.10.185
648   Long, D.T., Voice, T.C., Xagararoaki, I., Chen, A., Wu, H., Lee, E., Oun, A., Xing, F., 2017. Patterns of c-q
649   hysteresis loops and within an integrative pollutograph for selected inorganic and organic solutes
650   and E. coli in an urban salted watershed during winter-early spring periods. Appl. Geochem. 83,
651   93–107. https://doi.org/10.1016/j.apgeochem.2017.03.002
652   Lušić, D.V., Jozić, S., Cenov, A., Glad, M., Bulić, M., Lušić, D., 2016. Escherichia coli in marine water:
653   Comparison of methods for the assessment of recreational bathing water samples. Mar. Pollut.
654   Bull. 113, 438–443. https://doi.org/10.1016/j.marpolbul.2016.10.044
655   Martinez, J.M., Guyot, J.L., Filizola, N., Sondag, F., 2009. Increase in suspended sediment discharge of the
656   Amazon River assessed by monitoring network and satellite data. Catena 79, 257–264.
657   https://doi.org/10.1016/j.catena.2009.05.011
658   McKergow, L.A., Davies-Colley, R.J., 2010. Stormflow dynamics and loads of *Escherichia coli* in a large
659   mixed land use catchment. Hydrol. Process. 24, 276–289. https://doi.org/10.1002/hyp.7480
660   Mügler, C., Ribolzi, O., Janeau, J.-L., Rochelle-Newall, E., Latsachack, K., Thammahacksa, C., Viguier, M.,
661   Jardé, E., Henri-Des-Tureaux, T., Sengtaheuanghoung, O., Valentin, C., 2019. Experimental and
662   modelling evidence of short-term effect of raindrop impact on hydraulic conductivity and
663   overland flow intensity. J. Hydrol. 570, 401–410. https://doi.org/10.1016/j.jhydrol.2018.12.046
664   Navratil, O., Esteves, M., Legout, C., Gratiot, N., Nemery, J., Willmore, S., Grangeon, T., 2011. Global
665   uncertainty analysis of suspended sediment monitoring using turbidimeter in a small
666   mountainous river catchment. J. Hydrol. 398, 246–259.
667   https://doi.org/10.1016/j.jhydrol.2010.12.025
668   Nguyen, H.T.M., Le, Q.T.P., Garnier, J., Janeau, J.-L., Rochelle-Newall, E., 2016. Seasonal variability of
669   faecal indicator bacteria numbers and die-off rates in the Red River basin, North Viet Nam. Sci.
670   Rep. 6, 21644. https://doi.org/10.1038/srep21644
671   Oliver, D.M., Clegg, C.D., Heathwaite, A.L., Haygarth, P.M., 2007. Preferential Attachment of Escherichia
672   coli to Different Particle Size Fractions of an Agricultural Grassland Soil. Water. Air. Soil Pollut.
673   185, 369–375. https://doi.org/10.1007/s11270-007-9451-8
674   Pachepsky, Y., Stocker, M., Saldaña, M.O., Shelton, D., 2017. Enrichment of stream water with fecal
675   indicator organisms during baseflow periods. Environ. Monit. Assess. 189, 51.
676   https://doi.org/10.1007/s10661-016-5763-8
677   Pachepsky, Y.A., Allende, A., Boithias, L., Cho, K., Jamieson, R., Hofstra, N., Molina, M., 2018. Microbial
678   Water Quality: Monitoring and Modeling. J. Environ. Qual. 47, 931–938.
679   https://doi.org/10.2134/jeq2018.07.0277

680   Park, Y., Pachepsky, Y., Hong, E.-M., Shelton, D., Coppock, C., 2017. Release from Streambed to Water
681   Column during Baseflow Periods: A Modeling Study. J. Environ. Qual. 46, 219–226.
682   https://doi.org/10.2134/jeq2016.03.0114
683   Patin, J., Mouche, E., Ribolzi, O., Chaplot, V., Sengtahevanghoung, O., Latsachak, K.O., Soulileuth, B.,
684   Valentin, C., 2012. Analysis of runoff production at the plot scale during a long-term survey of a
685   small agricultural catchment in Lao PDR. J. Hydrol. 426–427, 79–92.
686   https://doi.org/10.1016/j.jhydrol.2012.01.015
687   Patin, J., Mouche, E., Ribolzi, O., Sengtahevanghoung, O., Latsachak, K.O., Soulileuth, B., Chaplot, V.,
688   Valentin, C., 2018. Effect of land use on interrill erosion in a montane catchment of Northern
689   Laos: An analysis based on a pluri-annual runoff and soil loss database. J. Hydrol. 563, 480–494.
690   https://doi.org/10.1016/j.jhydrol.2018.05.044
691   Ribolzi, O., Evrard, O., Huon, S., de Rouw, A., Silvera, N., Latsachack, K.O., Soulileuth, B., Lefèvre, I.,
692   Pierret, A., Lacombe, G., Sengtaheuanghoung, O., Valentin, C., 2017. From shifting cultivation to
693   teak plantation: effect on overland flow and sediment yield in a montane tropical catchment. Sci.
694   Rep. 7, 3987. https://doi.org/10.1038/s41598-017-04385-2
695   Ribolzi, O., Evrard, O., Huon, S., Rochelle-Newall, E., Henri-des-Tureaux, T., Silvera, N., Thammahacksac,
696   C., Sengtaheuanghoung, O., 2016a. Use of fallout radionuclides (7Be, 210Pb) to estimate
697   resuspension of Escherichia coli from streambed sediments during floods in a tropical montane
698   catchment. Environ. Sci. Pollut. Res. 23, 3427–3435. https://doi.org/10.1007/s11356-015-5595-z
699   Ribolzi, O., Lacombe, G., Pierret, A., Robain, H., Sounyafong, P., de Rouw, A., Soulileuth, B., Mouche, E.,
700   Huon, S., Silvera, N., Latxachak, K.O., Sengtaheuanghoung, O., Valentin, C., 2018. Interacting land
701   use and soil surface dynamics control groundwater outflow in a montane catchment of the lower
702   Mekong basin. Agric. Ecosyst. Environ. 268, 90–102. https://doi.org/10.1016/j.agee.2018.09.005
703   Ribolzi, O., Patin, J., Bresson, L.M., Latsachack, K.O., Mouche, E., Sengtaheuanghoung, O., Silvera, N.,
704   Thiébaux, J.P., Valentin, C., 2011. Impact of slope gradient on soil surface features and
705   infiltration on steep slopes in northern Laos. Geomorphology 127, 53–63.
706   https://doi.org/10.1016/j.geomorph.2010.12.004
707   Ribolzi, O., Rochelle-Newall, E., Dittrich, S., Auda, Y., Newton, P.N., Rattanavong, S., Knappik, M.,
708   Soulileuth, B., Sengtaheuanghoung, O., Dance, D.A.B., Pierret, A., 2016b. Land use and soil type
709   determine the presence of the pathogen Burkholderia pseudomallei in tropical rivers. Environ.
710   Sci. Pollut. Res. 23, 7828–7839. https://doi.org/10.1007/s11356-015-5943-z
711   Ribolzi, O., Silvera, N., Xayyakummanh, K., Latchachak, K., Tasaketh, S., Vanethongkham, K., 2005. The
712   use of pH to spot groundwater inflows along the stream of a cultivated catchment in the
713   northern Lao PDR. Lao J. Agric. For. 10, 72–84.
714   Robert, E., Grippa, M., Kergoat, L., Pinet, S., Gal, L., Cochonneau, G., Martinez, J.-M., 2016. Monitoring
715   water turbidity and surface suspended sediment concentration of the Bagre Reservoir (Burkina
716   Faso) using MODIS and field reflectance data. Int. J. Appl. Earth Obs. Geoinformation 52, 243–
717   251. https://doi.org/10.1016/j.jag.2016.06.016
718   Robert, E., Kergoat, L., Soumaguel, N., Merlet, S., Martinez, J.-M., Diawara, M., Grippa, M., 2017. Analysis
719   of Suspended Particulate Matter and Its Drivers in Sahelian Ponds and Lakes by Remote Sensing
720   (Landsat and MODIS): Gourma Region, Mali. Remote Sens. 9, 1272.
721   https://doi.org/10.3390/rs9121272
722   Rochelle-Newall, E., Nguyen, T.M.H., Le, T.P.Q., Sengtaheuanghoung, O., Ribolzi, O., 2015. A short review
723   of fecal indicator bacteria in tropical aquatic ecosystems: knowledge gaps and future directions.
724   Front. Microbiol. 6, 308. https://doi.org/10.3389/fmicb.2015.00308
725   Rochelle-Newall, E.J., Ribolzi, O., Viguier, M., Thammahacksa, C., Silvera, N., Latsachack, K., Dinh, R.P.,
726   Naporn, P., Sy, H.T., Soulileuth, B., Hmaimum, N., Sisouvanh, P., Robain, H., Janeau, J.-L.,
727   Valentin, C., Boithias, L., Pierret, A., 2016. Effect of land use and hydrological processes on

728   Escherichia coli concentrations in streams of tropical, humid headwater catchments. Sci. Rep. 6,
729   32974. https://doi.org/10.1038/srep32974

730 Smith, J., Edwards, J., Hilger, H., Steck, T.R., 2008. Sediment can be a reservoir for coliform bacteria
731   released into streams. J. Gen. Appl. Microbiol. 54, 173–179.
732   https://doi.org/10.2323/jgam.54.173

733 Song, L., Boithias, L., Sengtaheuanghoung, O., Oeurng, C., Valentin, C., Souksavath, B., Sounyafong, P., de
734   Rouw, A., Soulileuth, B., Silvera, N., Lattanavongkot, B., Pierret, A., Ribolzi, O., 2020. Understory
735   Limits Surface Runoff and Soil Loss in Teak Tree Plantations of Northern Lao PDR. Water 12,
736   2327. https://doi.org/10.3390/w12092327

737 Soupir, M.L., Mostaghimi, S., Dillaha, T., 2010. Attachment of *Escherichia coli* and Enterococci to Particles
738   in Runoff. J. Environ. Qual. 39, 1019–1027. https://doi.org/10.2134/jeq2009.0296

739 Stocker, M.D., Penrose, M., Pachepsky, Y.A., 2018. Spatial Patterns of Concentrations in Sediment before
740   and after High-Flow Events in a First-Order Creek. J. Environ. Qual. 47, 958–966.
741   https://doi.org/10.2134/jeq2017.11.0451

742 Strauch, A.M., Mackenzie, R.A., Bruland, G.L., Tingley, R., Giardina, C.P., 2014. Climate Change and Land
743   Use Drivers of Fecal Bacteria in Tropical Hawaiian Rivers. J. Environ. Qual. 43, 1475–1483.
744   https://doi.org/10.2134/jeq2014.01.0025

745 Tong, Y., Yao, R., He, W., Zhou, F., Chen, C., Liu, X., Lu, Y., Zhang, W., Wang, X., Lin, Y., Zhou, M., 2016.
746   Impacts of sanitation upgrading to the decrease of fecal coliforms entering into the environment
747   in China. Environ. Res. 149, 57–65. https://doi.org/10.1016/j.envres.2016.05.009

748 Troeger, C., Forouzanfar, M., Rao, P.C., 65 other authors, 2017. Estimates of global, regional, and
749   national morbidity, mortality, and aetiologies of diarrhoeal diseases: a systematic analysis for the
750   Global Burden of Disease Study 2015. Lancet Infect. Dis. 17, 909–948.
751   https://doi.org/10.1016/S1473-3099(17)30276-1

752 Turkelboom, F., Poesen, J., Trébuil, G., 2008. The multiple land degradation effects caused by land-use
753   intensification in tropical steeplands: A catchment study from northern Thailand. Catena 75,
754   102–116. https://doi.org/10.1016/j.catena.2008.04.012

755 Vigiak, O., Ribolzi, O., Pierret, A., Sengtaheuanghoung, O., Valentin, C., 2008. Trapping Efficiencies of
756   Cultivated and Natural Riparian Vegetation of Northern Laos. J. Environ. Qual. 37, 889–897.
757   https://doi.org/10.2134/jeq2007.0251

758 Wohlsen, T., Bates, J., Vesey, G., Robinson, W.A., Katouli, M., 2006. Evaluation of the methods for
759   enumerating coliform bacteria from water samples using precise reference standards. Lett. Appl.
760   Microbiol. 42, 350–356. https://doi.org/10.1111/j.1472-765X.2006.01854.x

761 Wold, S., 1995. PLS for Multivariate Linear Modelling. In: van de Waterbeemd H. (ed.), QSAR:
762   Chemometric Methods in Molecular Design. Vol 2. Wiley-VCH, Weinheim, Germany. pp. 195–
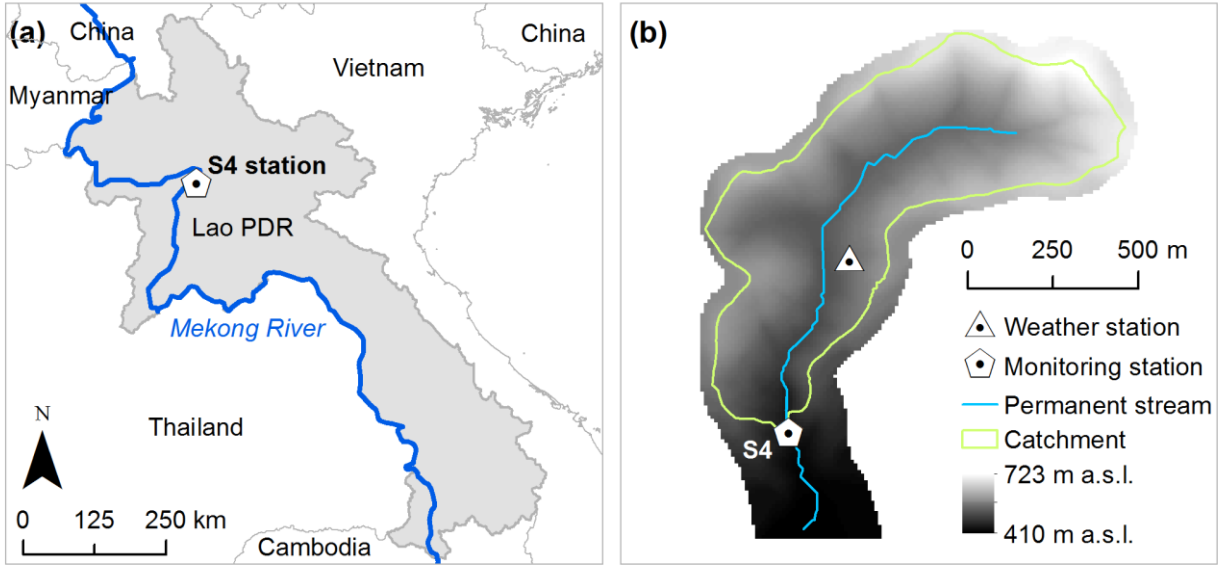763   218.

764 Ziegler, A.D., Benner, S.G., Tantasirin, C., Wood, S.H., Sutherland, R.A., Sidle, R.C., Jachowski, N., Nullet,
765   M.A., Xi, L.X., Snidvongs, A., Giambelluca, T.W., Fox, J.M., 2014. Turbidity-based sediment
766   monitoring in northern Thailand: Hysteresis, variability, and uncertainty. J. Hydrol. 519, 2020–
767   2039. https://doi.org/10.1016/j.jhydrol.2014.09.010

768 Ziegler, A.D., Giambelluca, T.W., Tran, L.T., Vana, T.T., Nullet, M.A., Fox, J., Vien, T.D., Pinthong, J.,
769   Maxwell, J.., Evett, S., 2004. Hydrological consequences of landscape fragmentation in
770   mountainous northern Vietnam: evidence of accelerated overland flow generation. J. Hydrol.
771   287, 124–146. https://doi.org/10.1016/j.jhydrol.2003.09.027
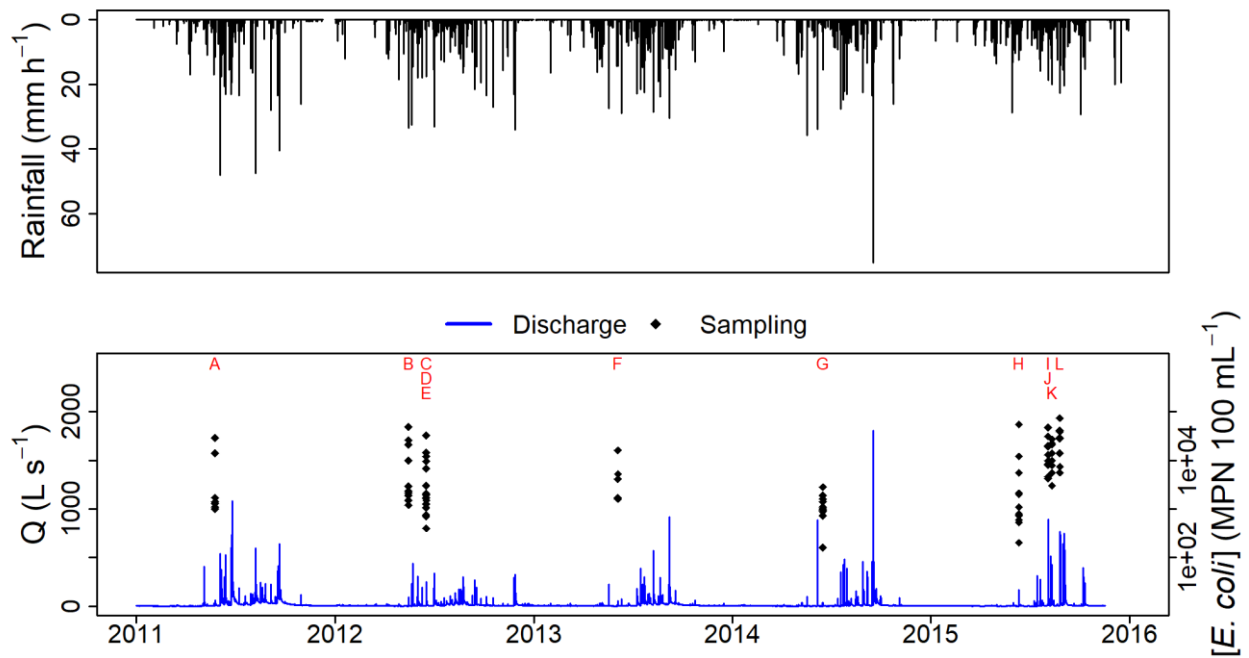
772

773

775

776

777   Fig. 1. (a) Location of the S4 outlet of the Houay Pano catchment in northern Lao PDR; (b) River gauging

778   and sampling station S4, weather station, and altitudes. Altitudes are given in meters above sea level (m
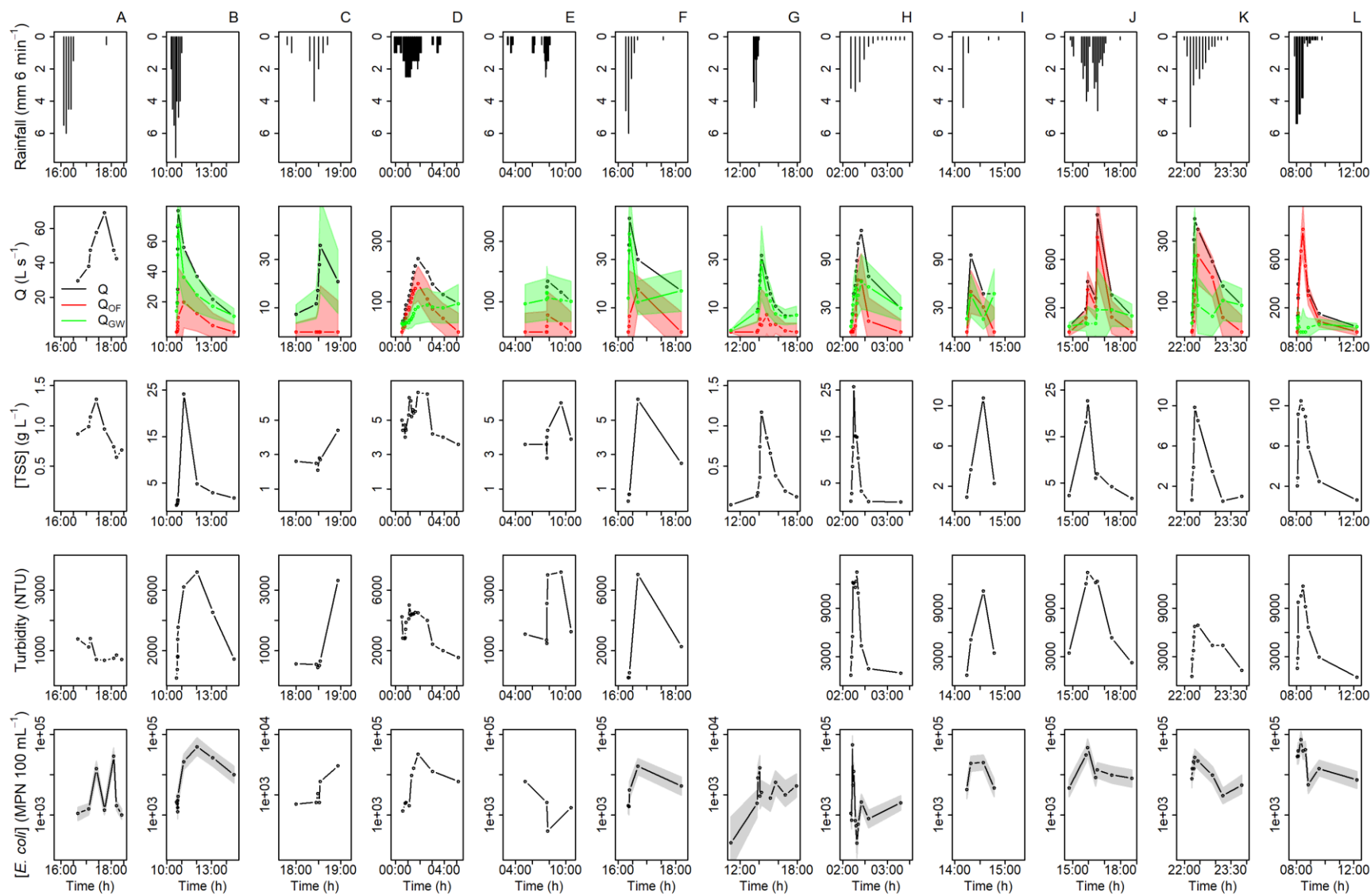
779   a.s.l.).

780

781

782

783

784

785   Fig. 2. Rainfall (mm h^{-1}) and discharge (Q, in L s^{-1}) for the 2011-2015 period, and *E. coli* concentration ([*E.*

786   *coli*], in MPN 100 mL^{-1}) for twelve flood events from 2011 to 2015 at the outlet of the Houay Pano

787   catchment, northern Lao PDR. The flood events of 16-17 June 2012 (C, D, and E) and of 4 August 2015 (I

788   and J) have been decomposed into 3 and 2 separate flood events. Details of these two flood events is

789   shown in Fig. 3. Although [*E. coli*] measures for events C-E were expressed in CFU 100 mL^{-1}, they are

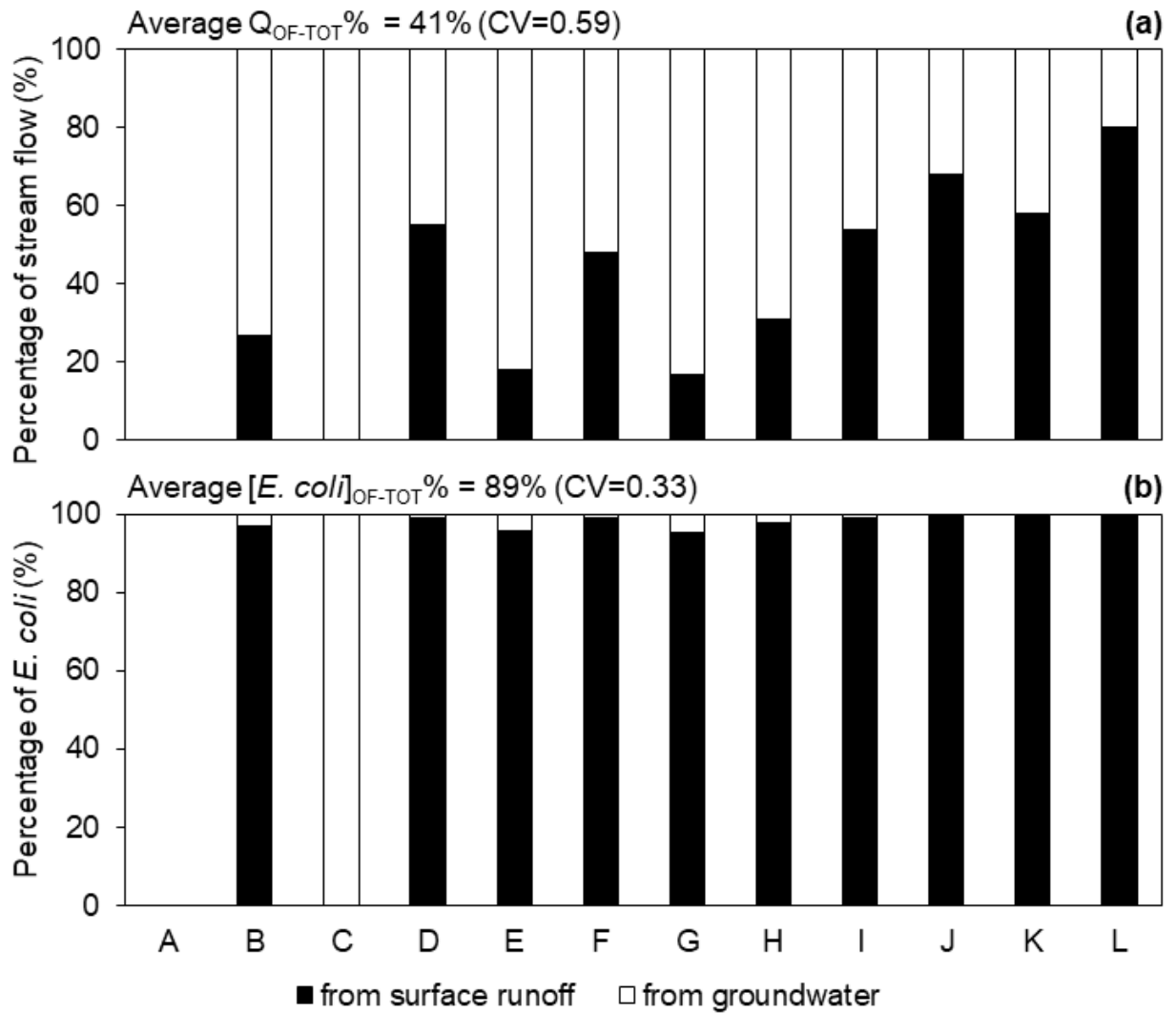790   reported as MPN 100 mL^{-1} for the sake of simplicity.

791

793   Fig. 3. Monitored flood events from 2011 to 2015 at the outlet of the Houay Pano catchment, northern Lao PDR. Rainfall: rainfall (mm); Q:

794   discharge (L s^{-1}); Q$_{OF}$: surface runoff (L s^{-1}); Q$_{GW}$: sub-surface flow (L s^{-1}); [TSS]: total suspended sediments concentration (g L^{-1}); Turbidity: turbidity

795   (NTU); [*E. coli*]: *E. coli* concentration (MPN 100 mL^{-1}). Measurements of turbidity were lacking for event G. Although [*E. coli*] measures for events

796   C-E were expressed in CFU 100 mL^{-1}, they are reported as MPN 100 mL^{-1} for the sake of simplicity. Red and green bands for Q$_{OF}$ and Q$_{GW}$,

797   respectively, are uncertainty bands calculated with the Genereux (1998) method. Grey bands for [*E. coli*] are uncertainty intervals given by

798   Poisson distribution when using the standardized microplate method.

799

Fig. 4. Contributions (in %) of overland flow and of groundwater flow in (a) flood-event total volume of stream flow, and in (b) flood-event total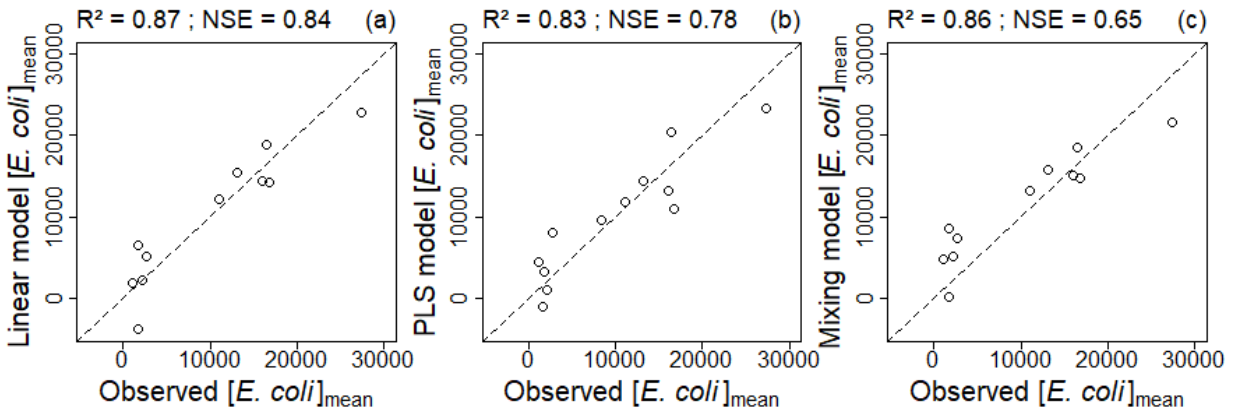 *E. coli* number. The twelve flood events were sampled from 2011 to 2015 at the outlet of the Houay Pano catchment, northern Lao PDR. Measurements of electrical conductivity were missing for event A. Average $Q_{OF\text{-}TOT}$% and average $[E.\ coli]_{OF\text{-}TOT}$% are the average contribution of overland flow to the 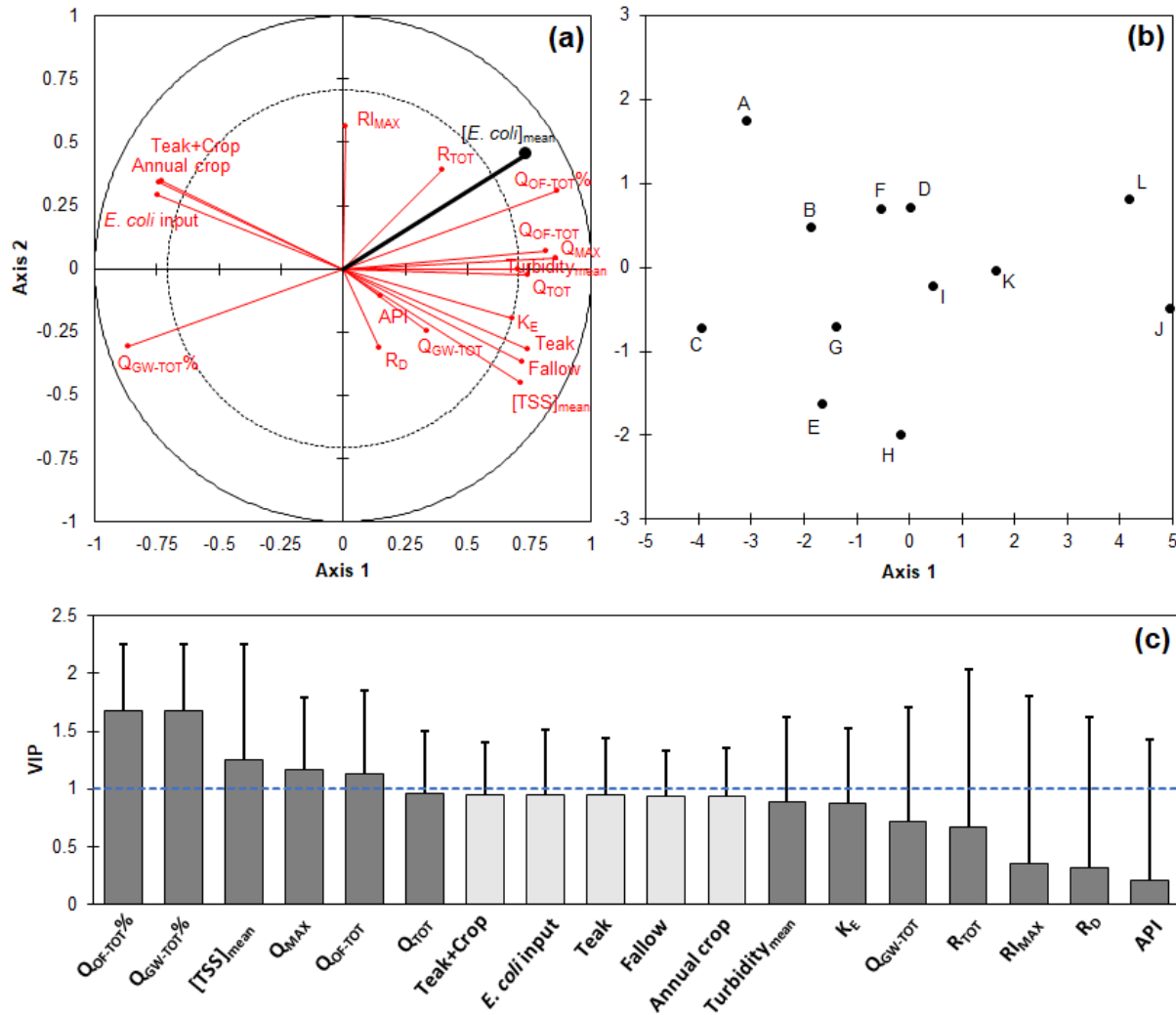in-stream flow and the average percentage of *E. coli* resulting from overland flow, respectively. CV: coefficient of variation.

808

809 Fig. 5. Mean *E. coli* concentration per flood event ([*E. coli*]$_{mean}$): comparison of models' predictions with

810 observed values (MPN 100 mL^{-1}). (a) Q$_{OF-TOT}$%-based linear model against observed [*E. coli*]$_{mean}$; (b) PLS

811 model against observed [*E. coli*]$_{mean}$; (c) Mixing model against observed [*E. coli*]$_{mean}$. R^2: coefficient of

812 determination; NSE: Nash-Sutcliffe Efficiency. The twelve flood events were sampled from 2011 to 2015

813 at the outlet of the Houay Pano catchment, northern Lao PDR.

814

Fig. 6. Partial Least Square regression analysis where the flood-event mean concentration of *E. coli* ([*E.*

coli]$_{mean}$) is explained by hydro-meteorological and land-use variables: (a) *E. coli* located in the

correlations circle with 13 meteorological and hydrological variables and 5 land-use variables; (b) Map of

observations (twelve flood events from 2011 to 2015 at the outlet of the Houay Pano catchment,

northern Lao PDR); (c) Variable Importance in Projection (VIP) of the 18 variables for two components.

R_D: event rainfall duration; R_{TOT}: cumulated rainfall over the event; RI_{MAX}: maximum rainfall intensity; API:

antecedent precipitation index; Q_{MAX}: peak discharge during the event; Q_{TOT}: total volume of stream

water exported during the event; Q_{OF-TOT}: total volume of surface runoff exported during the event; Q_{OF-}

$_{TOT}$%: percentage of surface runoff during the event calculated as $Q_{OF-TOT}/Q_{TOT}*100$; Q_{GW-TOT}: total volume

824   of sub-surface flow exported during the event; Q_{GW-TOT}%: percentage of sub-surface flow during the

825   event calculated as Q_{GW-TOT}/Q_{TOT}*100; K_E: flow coefficient calculated as Q_{TOT}/R_{TOT}; $[TSS]_{mean}$: flood-event

826   mean total suspended sediments concentration; $Turbidity_{mean}$: flood-event mean turbidity; Fallow:

827   annual percentage of the catchment area covered by fallow; Teak: annual percentage of the catchment

828   area covered by teak trees; Annual crop: annual percentage of the catchment area covered by annual

829   crops; Teak+Crop: annual percentage of the catchment area covered by annual crops grown under young

830   teak trees; *E. coli* input: monthly *E. coli* input within the catchment.

List of tables

Table 1. Hydro-meteorological characteristics of the selected flood events from 2011 to 2015 at the outlet of the Houay Pano catchment, northern Lao PDR.

Event	Start date Time	Rainfall R_D (min)	R_{TOT} (mm)	RI_{MAX} (mm h^{-1})	API (mm)	Discharge Q_{MAX} (L s^{-1})	Q_{TOT} (m^3)	Q_{OF-TOT} (m^3)	Q_{OF-TOT}% (%)	K_E (%)	n (-)	Water quality [TSS]$_{mean}$ (g L^{-1})	Turbidity$_{mean}$ (NTU)	[E. coli]$_{mean}$ (MPN 100 mL^{-1})
A	05/25/2011 16:06	24	22.5	60	15.5	69.1	305.5			2.3	8	1.0	993.6	8388
B	05/15/2012 10:18	42	33.5	75	2.8	80.3	553.4	146.7	27	2.7	10	4.9	5466.0	2672
C	06/16/2012 17:48	54	10.5	40	15.0	35.8	69.7	0.0	0	1.1	6	2.9	594.2	1682
D	06/17/2012 00:00	228	39	25	48.6	242.0	2620.8	1432.4	55	11.2	18	5.3	3252.9	16053
E	06/17/2012 03:00	306	19	25	40.6	168.4	2471.3	440.9	18	21.6	7	4.1	2578.0	2181
F	06/04/2013 16:11	82	14.6	60	12.3	47.0	215.6	103.3	48	2.5	5	2.0	5860.3	11020
G	06/16/2014 13:19	36	15.4	44	9.3	31.7	222.6	38.4	17	2.4	11	0.6		1125
H	06/12/2015 02:06	74	13.2	34	11.1	125.8	308.9	96.4	31	4.0	12	10.1	3696.0	1748
I	08/04/2015 13:22	50	6	44	4.3	95.2	127.4	69.1	54	3.8	4	4.8	6809.8	16776
J	08/04/2015 14:49	131	34.6	46	30.9	967.9	5554.2	3796.0	68	26.7	7	9.8	7790.9	16403
K	08/11/2015 21:59	81	20.8	56	17.4	374.7	1378.9	804.9	58	11.0	9	6.0	5205.8	13112
L	08/26/2015 07:48	116	32.4	54	16.2	849.6	3903.6	3118.3	80	20.0	10	8.2	4822.8	27375

R_D: duration of rainfall event; R_{TOT}: cumulated rainfall of the event; RI_{MAX}: maximum rainfall intensity; API: antecedent precipitation index; Q_{MAX}: peak discharge during the flood event; Q_{TOT}: total volume of stream water exported during the event; Q_{OF-TOT}: total volume of surface runoff exported during the event; Q_{OF-TOT}%: percentage of surface runoff during the event calculated as $Q_{OF-TOT}/Q_{TOT}*100$; K_E: flow coefficient calculated as Q_{TOT}/R_{TOT}; n: sample size; [TSS]$_{mean}$: flood-event mean total suspended sediments concentration; Turbidity$_{mean}$: flood-event mean turbidity; [E. coli]$_{mean}$: flood-event mean E. coli concentration. Measurements of EC and of Turbidity were lacking for events A and G, respectively. Although E. coli measurements for events C-E were expressed in CFU 100 mL^{-1}, they are reported as MPN 100 mL^{-1} for the sake of simplicity.